Icarus 264 (2016) 443–455

Contents lists available at ScienceDirect

Icarus

journal homepage: www.journals.elsevier.com/icarus

Consequences of a solid inner core on Mercury's spin configuration

Stanton J. Peale [a,1], Jean-Luc Margot [b,c,*], Steven A. Hauck, II [d], Sean C. Solomon [e,f]

[a] Department of Physics, University of California, Santa Barbara, CA 93106, United States
[b] Department of Earth, Planetary, and Space Sciences, University of California, Los Angeles, CA 90095, United States
[c] Department of Physics and Astronomy, University of California, Los Angeles, CA 90095, United States
[d] Department of Earth, Environmental, and Planetary Sciences, Case Western Reserve University, Cleveland, OH 44106, United States
[e] Department of Terrestrial Magnetism, Carnegie Institution of Washington, Washington, DC 20015, United States
[f] Lamont-Doherty Earth Observatory, Columbia University, Palisades, NY 10964, United States

ARTICLE INFO

Article history:
Received 12 May 2015
Revised 14 September 2015
Accepted 16 September 2015
Available online 1 October 2015

Keywords:
Rotational dynamics
Mercury, interior
Planetary dynamics
Tides, solid body

ABSTRACT

The pressure torque by a liquid core that drove Mercury to the nominal Cassini state of rotation is dominated by the torque from the solid inner core. The gravitational torque exerted on Mercury's mantle from an asymmetric solid inner core increases the equilibrium obliquity of the mantle spin axis. Since the observed obliquity of the mantle must be compatible with the presence of a solid inner core, the moment of inertia inferred from the occupancy of the Cassini state must be reduced to compensate the torque from the inner core and bring Mercury's spin axis to the observed position. The unknown size and shape of the inner core means that the moment of inertia is more uncertain than previously inferred.

1. Introduction

Mercury is in a stable spin–orbit resonance in which the rotational angular velocity is precisely 1.5 times the mean orbital motion (Pettengill and Dyce, 1965; Colombo and Shapiro, 1966). This rotation state is a natural outcome of tidal evolution (Goldreich and Peale, 1966) or other dissipative effects, although the details of the resonance capture mechanism are still debated (Correia and Laskar, 2004, 2009, 2012; Wieczorek et al., 2012; Noyelles et al., 2014). In addition, the same dissipation brings Mercury to Cassini state 1, wherein Mercury's spin axis remains coplanar with the orbit normal and Laplace plane normal as the spin vector and orbit normal precess around the latter with a ~300,000 yr period (Colombo, 1966; Peale, 1969, 1974). Because the Laplace plane is itself variable on long time scales, one can invoke an instantaneous Laplace plane that is valid at the present epoch (Yseboodt and Margot, 2006). On the basis of theoretical calculations, Mercury is expected to remain close to the Cassini state (Peale, 2006). That Mercury is very close to this state has been verified with radar observations, which give an obliquity of 2.04 ± 0.08 arcmin (Margot et al., 2007, 2012), consistent with analysis of tracking data, laser altimetry, and stereo digital terrain models from the MErcury Surface, Space ENvironment, GEochemistry, and Ranging (MESSENGER) spacecraft (Mazarico et al., 2014; Stark et al., 2015). The most recent observations show that the best-fit solutions are offset from the Cassini state by a few arcseconds, but the uncertainty at one standard deviation includes the Cassini state.

Pressure torque between Mercury's fluid core and its mantle drive Mercury's spin axis to the Cassini state (Peale et al., 2014) (hereinafter Paper 1). It thereby dominates dissipative viscous, topographic, and magnetic effects that would otherwise result in significant displacement of the observable spin axis from the Cassini state position. This result is reassuring as Mercury's spin is observed to occupy the Cassini state (Margot et al., 2007, 2012; Mazarico et al., 2014; Stark et al., 2015), but at the same time it frustrates the establishment of any constraints on Mercury's interior that could result from a measurable displacement. We show here that the increase in the obliquity from torques exerted by an asymmetric solid inner core can be reversed by the reduction of Mercury's polar moment of inertia from the value inferred if there is no inner core. For a small inner core, the current best estimate of the moment of inertia would be unchanged, but for a large inner core, the revised estimate would be smaller than the current estimate.

The assumed model of the planet consists of four homogeneous layers: crust, mantle, fluid outer core, and solid inner core (Fig. 1). R_i and ρ_i designate the radii and densities of the various layers, with subscript c for crust, m for mantle, f for fluid outer core, and s for solid inner core. $R_e = 2440$ km is the measured planetary radius,

* Corresponding author at: Department of Earth, Planetary, and Space Sciences, University of California, Los Angeles, CA 90095, United States.
E-mail address: jlm@epss.ucla.edu (J.-L. Margot).
[1] Deceased 14 May 2015.

http://dx.doi.org/10.1016/j.icarus.2015.09.024
0019-1035/

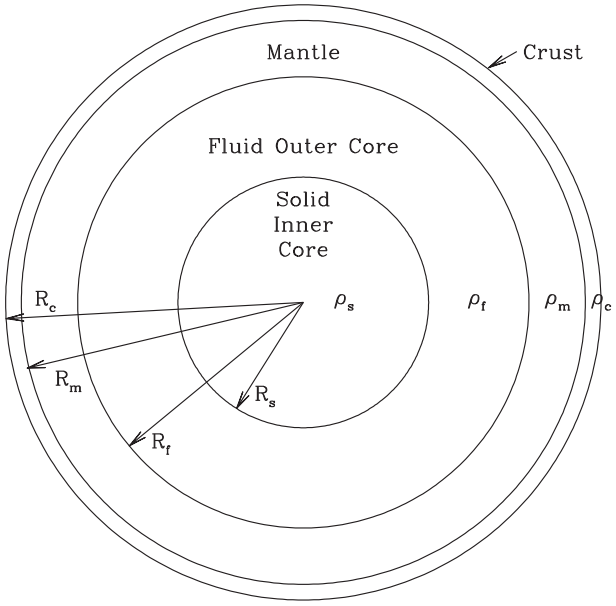

Fig. 1. Model of Mercury's interior as four concentric and homogeneous layers. Note that in our notation R_c is the radius of the crust, which is that of the planet. This symbol is often used in other publications to indicate the radius of the fluid core, which in our notation is R_f. We assume $R_c = 2440$ km and $\rho_c = 2.8$ g/cm^3 in all our calculations.

and the selected value of ρ_c is described below. The crustal thickness is specified by the choice of R_m. The inner core ρ_s and R_s are also specified, as follows. We will evolve the spin configuration for three values of ρ_s (8.0, 9.3, and 10.0 g/cm^3) to span the uncertainty in this value. Five inner core radii will be assumed (0.0 or no inner core, 0.3, 0.4, 0.5, and 0.6 R_c, where R_c should not be confused with R_f). The densities ρ_f, ρ_m along with the radius R_f of the core–mantle boundary (CMB) will be solved to produce the known values of the total planetary mass m, the total moment of inertia C/mR_c^2, and the moment of inertia of the mantle–crust alone $(C_m + C_c)/C$.

The second-degree zonal and tesseral spherical harmonic gravitational coefficients J_2 and C_{22} can be expressed in terms of the densities and radii of the layers and their ellipticities. The ellipticities of the top of the crust have been measured; the mean polar ellipticity $\epsilon_c = 5.534 \times 10^{-4}$ and the equatorial ellipticity $\xi_c = 4.919 \times 10^{-4}$ (Perry et al., 2015). Expressions for J_2 and C_{22} along with relations for the assumed equipotential surfaces at the CMB and inner core boundary (ICB) provide a sufficient number of equations to solve for all the remaining ellipticities, which change with a change in the assumed inner core radius. The ellipticities are required to calculate the torques. We will neglect the $\sim 15^\circ$ misalignment of the equatorial long axis and the $\sim 2^\circ$ misalignment of the short axis of the crust with those of the geoid as determined by MESSENGER laser altimetry and radio occultations (Perry et al., 2015).

In Section 2 we write the general dynamical equations that are derived in Paper 1. Although written for the mantle–crust combination, they apply to the other two layers representing the fluid core and the solid inner core with a change in the subscripts of the parameters. There are three sets of equations that must be solved simultaneously to map the evolution of the system of equations for the combined crust and mantle and the outer and inner core to the equilibrium configuration. The various torques to be used in the equations are developed in several subsections. The ICB will be at least gravitationally distorted by the non-radial internal field of the mantle–crust and fluid outer core and less so by the solar and rotational fields (Paper 1). We include the mutual gravitational torques that result from any misalignment of the ellipsoidal shape of the inner core with that of the mantle. This torque is sustained since the inner core obliquity remains larger than the mantle obliquity in equilibrium. We consider this mutual torque along with the direct solar gravitational torques acting on each of the three layers, the mantle–crust, the fluid outer core, and the solid inner core. The first is considered a single layer for the dynamical equations, since mantle and crust move together. Pressure torques acting at the CMB and at the ICB include those induced by gravity and by the fluid velocity at the ICB and CMB. A viscous interaction provides a dissipative evolution to an equilibrium configuration whereby the spin axes of the respective layers remain fixed in a frame precessing with the orbit. The torques from tides, magnetic coupling, and topographic coupling treated in Paper 1 are small and do not affect the evolution to the equilibrium state. These latter torques are therefore not included here.

We chose a crustal density $\rho_c = 2.8$ g/cm^3, which we maintain for all of the calculations. This choice is based on results from the Moon, where the mean crustal density is 2.6 g/cm^3, which implies considerable porosity (12%) (Wieczorek et al., 2013). The lunar crustal density approaches 2.4 g/cm^3 at the shallowest depths. The 2.8 g/cm^3 chosen for Mercury's crust can then account for Mercury's higher surface gravitational acceleration and perhaps a lower porosity. The inner core density is arbitrary except that $\rho_s = 8$ g/cm^3 is taken as a lower limit to possible values. That the mantle–crust obliquity decreases with C/mR_c^2 suggests that by reducing C/mR_c^2 we can compensate for the increased obliquity caused by the interaction between the mantle–crust and the inner core. When the moment of inertia is that which is appropriate for no inner core, the mantle obliquity is displaced to larger and larger obliquities as the inner core size increases. The mantle obliquity is matched to within the observational uncertainty by appropriate reductions in C/mR_c^2 for each core size. These reductions increase as the inner core size increases. Some of the models obtained for the range of inner core densities are unlikely.

The results are detailed in Section 3 for the ranges of inner core sizes and densities considered. We show that for an ICB and a CMB that are equipotential surfaces, the equilibrium position of the mantle spin is displaced toward obliquities higher than that of the Cassini state appropriate to Mercury with no solid inner core and therefore higher than the observed obliquity. We demonstrate below that the required reductions in C/mR_c^2 are significant for $R_s > 0.3R_c$. The displacement of the evolved mantle spins from the Cassini state for the unaltered $C/mR_c^2 = 0.346$ determined from the observed obliquity and deduced for Mercury with a fluid core but no solid inner core is shown for $\rho_s = 8.0$ g/cm^3 only. The restoration of the evolved mantle-crust spin to the observed position for all three inner core densities is shown with appropriate reductions in C/mR_c^2.

The mantle–crust obliquity increases with the inner core size. The displacement vanishes if the direct gravitational torque between the mantle and inner core is set to zero. The obliquity is used to determine the moment of inertia of Mercury (e.g., Peale et al., 2014). The increase in the obliquity of the mantle from gravitational torques due to the inner core means that C/mR_c^2 must be reduced by an amount that increases with inner core radius to bring the mantle spin back to the observed position. We discuss the implications in Section 4 where the values of C/mR_c^2 versus R_s, the radius of the solid inner core, are given. This exercise is repeated for inner core densities of 9.3 g/cm^3 and 10.0 g/cm^3.

2. Equations of variation

The coordinate systems and angles for the equations that govern the rotational motion of Mercury are shown in Fig. 2, where X', Y', Z' are quasi-inertial axes with the $X'Y'$ plane being the